Embedded and Controllable Shape Morphing with Twisted-and-Coiled Actuators*

Jiefeng Sun[1], Ben Pawlowski[1], and Jianguo Zhao[1]

Abstract—Shape morphing, meaning a structure can first morph and then lock into another shape, can be applied to robot designs to endow robots with adaptive morphology for increased functionality and adaptivity. In this paper, we introduce a novel shape morphing scheme enabled by a new artificial muscle: twisted and coiled actuators (TCAs). This new actuator is purely soft, low cost, and electrically driven. Embedding a TCA and a thermoplastic material with variable stiffness into soft materials, we create a miniature shape-morphing link. We also establish a general model to predict the steady-state shape of the link given an input power applied to the TCA. Experiments are conducted to characterize parameters and verify the proposed model. Finally, we demonstrate this shape-morphing link can serve as a link in a mechanism to change the trajectory of its foot or endpoint. We envision that such a new shape-morphing scheme can enable robots to leverage the same mechanical design for different functions.

I. INTRODUCTION

Shape morphing means a structure can first morph and then lock into another shape without additional energy input. It has many promising applications including human-machine interface, deployable structures, self-assembly, and in particular, robotics [1]. Robots with shape morphing capabilities can leverage the same mechanical mechanism to locomote in different environments or extend their dynamic envelopes. Examples include aircraft with morphing wings that can successfully maneuver to land on a human hand with improved dynamics performance [2].

A structure with shape morphing capabilities should have two essential elements: 1) controllable stiffness, so it can be rigid before and after the shape change and soft in-between; 2) an actuator to provide sufficient force and displacement to achieve the desired shape. In the following, we briefly review existing work on these two elements.

Variable stiffness elements have been investigated extensively in recent years. Stiffness tuning between soft and rigid is conventionally achieved in a system level by the variable stiffness of mechanisms [3]. However, it can be more easily achieved at a material level through the use of thermally responsive materials such as shape memory polymers (SMP), conductive elastomer, phase-changing alloys, or low-melting point alloys (LMPA). However, these materials are often subject to complicated fabrication processes [4] or require

either high current [5] or high voltage [6], limiting their applications in robots of small sizes.

In this paper, we leverage thermoplastic materials with low glass transition temperatures for the variable stiffness element [7]. Compared with other variable stiffness approaches, thermoplastic materials can be purchased off-the-shelf at a low cost and only require a heating element for stiffness control. Among thermoplastic materials, we choose polylactide (PLA) because it has a low glass transition temperature ($\sim 62°$C) and high stiffness (1.7 GPa) [8].

For actuation, researchers often turn to artificial muscles, tendons, or controllable fluids. Shape memory alloy (SMA) has been widely used for actuation to enable shape morphing. Tendons driven by external motors have also been widely used to achieve reliable, cheap, and easy control of soft body for shape morphing, but electrical motors, stiff and heavy, might limit bending or shape changing of the soft body[9]. Hydraulic or pneumatic actuation based on modular inflatable chambers can generate relatively larger forces and faster responses, but they require external parts to generate pressure, restricting their applications in small robots[10].

In this paper, we leverage a new artificial muscle, twisted and coiled actuators (TCAs) [11], for the actuation of shape morphing. TCAs have distinctive advantages compared with existing artificial muscles [12]. First, they are low cost because of commercially available, inexpensive fishing line or sewing threads. Second, TCAs can contract up to 49% and generate forces 100 times larger than a human muscle of the same weight and length [11].

In this paper, we introduce a new shape-morphing scheme comprised of a soft body embedded with a PLA rod for variable stiffness and a TCA for actuation. The general shape morphing process can be divided into three steps as shown in Fig. 1: (1) a voltage is applied to a resistive wire wrapped around the PLA to soften the PLA (from (a) to (b)); (2) once the PLA becomes soft, the heating is turned off, and the TCA is actuated to bend the structure (from (b) to (c)); (3) after the structure achieves a specific shape, the TCA is controlled to maintain that shape until the soft PLA becomes rigid (from (d) to (e)).

The main contributions of this paper are as follows. First, we propose a novel shape-morphing scheme enabled by TCAs. Second, we establish and experimentally verify mathematical models to predict the final shape given the power applied to TCA for a shape-morphing link. Such a model will lay a foundation for precisely controlling the morphed shape. Third, we apply the shape-morphing link to a four-bar linkage to alter the linkage's trajectory. Such a preliminary
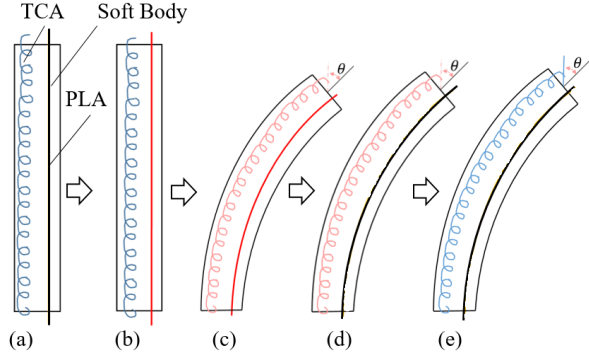
Fig. 1: Morphing process of a shape-morphing link. (a) Initial configuration. (b) The variable stiffness element PLA is heated up and becomes soft. (c) Activate the TCA. (d) The PLA becomes rigid. (e) Deactivate the TCA and the link holds its new configuration.

test will enable robots to leverage the same mechanical mechanisms for locomoting in different environments (e.g., hybrid aerial and aquatic robots with morphing wings for both flying and swimming).

The rest of this paper is organized as follows. In section II, we describe the mathematical model to predict the resulting shape given a power input applied to the TCA. In section III, we detail the materials and fabrication of the morphing link, and experiments conducted in water are elaborated to verify the proposed model. In section IV, we demonstrate that a four-bar linkage with the shape-morphing link can generate different foot trajectories.

II. MODELING

During the morphing process (Fig. 1(c)), different power applied to the TCA will generate different shapes for the shape-morphing link. In order to precisely control the morphing shape, we need to first establish mathematical models to predict the shape based on the power applied to the TCA. This can be divided into two steps. We first establish a thermal model to predict the steady-state temperature of the TCA from the input power. With the derived temperature as input, we then use a forward kinetostatic model to predict the shape of the shape-morphing link.

A. Thermal Model

The thermal model aims to relate the input power and the steady-state temperature of the TCA. Since the length of the shape-morphing link is much larger than its cross section dimensions, we can simplify this three-dimensional heat transfer problem into two dimensions by only considering temperature distribution on the cross section of the link, as shown in Fig. 2. The steady-state temperature distribution over the cross-section is governed by the following heat diffusion equation applied to each material [13]

$$\frac{\partial}{\partial x}\left(k\frac{\partial T}{\partial x}\right) + \frac{\partial}{\partial y}\left(k\frac{\partial T}{\partial y}\right) + \dot{q} = \rho c_p \frac{\partial T}{\partial t} \qquad (1)$$

where T is the temperature distribution throughout the material, $\dot{q}$ is heat flux of the material (i.e., $\dot{q}_T$ for the TCA and $\dot{q}_P$ for PLA), and t is time. k, ρ, and c_p are the thermal conductivity, mass density, and specific heat of the material, respectively.
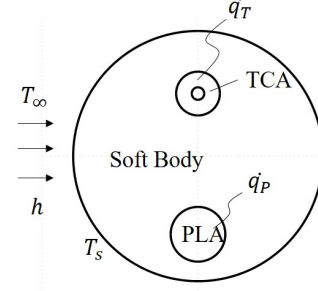

Fig. 2: Schematic of the thermal model.

The heat generated by the TCA comes from Joule heating, where a conductive material generates heat due to the applied electrical power. Although the electrical resistance of a TCA varies both with temperature [14] and force [15], we neglect these small changes. We also approximate the shape of the TCA as a tube by neglecting the small gaps between coils. Thus, the body heat flux of a TCA is [13]

$$\dot{q}_T = \frac{4U_T^2}{R_0 l^2 \pi \left(D^2 - d^2\right)} \qquad (2)$$

where U_T is the voltage applied to the TCA, R_0 is the resistance of a unit length of the TCA, l is the length of a single TCA, D and d are the outer and the inner diameters of the TCA, respectively.

We assume the PLA is uniformly heated by the power supplied to the resistance wire P_P. The heat flux through the PLA is then $\dot{q}_P = P_P/V_P$, where V_P is the volume of the PLA included in the soft body. We can then specify the convective boundary condition as the heat transfer along the perimeter of the circular cross section [13]

$$k\left(\frac{\partial T}{\partial x} + \frac{\partial T}{\partial y}\right) = h(T - T_\infty) \qquad (3)$$

where T is the temperature distribution on the boundary, T_∞ is ambient temperature, and h is convective heat transfer coefficient.

Since the temperature of the shape morphing link's surface is not very high ($< 100°C$), we can ignore energy loss from radiation. The TCA's temperature can be computed as the average temperature over the cross section of the TCA.

B. Forward Kinetostatics

With the temperature of the TCA, we can predict the geometry of the shape-morphing link using the forward kinetostatics of a soft rod and the actuation model of the TCA [16].

For the kinetostatics of a soft rod, we use a Cosserat Rod model [17]. A Cosserat model begins by treating the basic element of a body as an infinitesimal rigid body rather than

a point-particle. The rod form of the Cosserat model then assumes that the body is much longer than its width, thus the deformation only occurs along the length of the body and the cross-sections remain undeformed. This assumption makes the fundamental element of the Cosserat Rod model (Fig. 3) a rigid plane (the cross-sections of the body) and the one spatial dimension is the curve going from the base to the tip of the body and passing through the centroids of all the cross-sections. This curve, referred as the material abscissa, can be parametrized by a variable $s \in [0, L]$ where L is the length of the link in the reference configuration. With the rigid cross-sections, we can then attach orthonormal frames at their centroids, which are typically called the directors. We can define a rotation, R, and a position, p, between the fixed frame and the cross-sections, allowing us to describe the configuration of the individual planes and the total configuration of the body over s. The strains in the body can then be established as the change in the directors across s. The configuration is thus written as
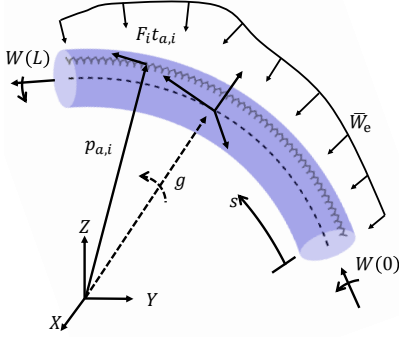

Fig. 3: Diagram for a Cosserat Rod. g represents the transformation from the fixed frame to the body frame. The internal wrench is W and the distributed wrench is $\bar{W}_e$. The force and the position in the TCA are represented by $F_i t_{a,i}$ and $p_{a,i}$. The variable s is the spatial parameter varying from 0 at the base to L at the tip.

$$\dot{g} = g\widehat{\boldsymbol{\xi}} = \begin{bmatrix} R & p \\ \mathbf{0} & 1 \end{bmatrix} \begin{bmatrix} \widehat{\boldsymbol{\omega}} & \boldsymbol{\nu} \\ \mathbf{0} & 0 \end{bmatrix} \tag{4}$$

where the operator $\dot{}$ represents the derivative with respect to s, g is the homogeneous transformation matrix from the fixed frame to the directors, $\boldsymbol{\xi} = [\boldsymbol{\omega}, \boldsymbol{\nu}]^T$ is the strain vector or spatial twist composed of the angular strain, $\boldsymbol{\omega}$, and the linear strain, $\boldsymbol{\nu}$. The operator $\widehat{}$ is the transformation from $\mathbb{R}^3$ to $se(3)$. Another operator $\check{}$ will also be used later to represent the inverse transformation from $se(3)$ to $\mathbb{R}^3$. Both $\widehat{}$ and $\check{}$ can also represent transformations between $SE(3)$ and $\mathbb{R}^6$.

We can assume that the shape-morphing link will experience a constant strain along the body. This is reasonable since we will experimentally verify the shape morphing in water to speed up the heat transfer process. In water, the external forces: gravity force and buoyancy force will balance, and the TCA apply a constant force across the body. With a constant

strain assumption, the transformation matrix g can be written as

$$g = g_0 e^{\widehat{\boldsymbol{\xi}} s} \tag{5}$$

Next, we consider the static equilibrium to determine the strain. At equilibrium the internal wrench from the stiffness of the body, W_{int}, and the applied wrench from the actuator, W_{act}, should balance, $W_{int} = W_{act}$. A wrench is the combination of a moment and force, i.e., $W = [M, F]^T$.

The actuator wrench is determined by the force and moment generated by the TCA in the fixed frame and then transforming it into the director frame. The generated force can be computed from the temperature and the length through the TCA model in [16].

$$W_{act} = Ad_g^* \begin{bmatrix} \widehat{p}_a F(\delta, q) t_a \\ F(\delta, q) t_a \end{bmatrix} = F \begin{bmatrix} \widehat{r} R^T t_a \\ R^T t_a \end{bmatrix} \tag{6}$$

$$Ad_g^* = \begin{bmatrix} R^T & R^T \widehat{p}^T \\ 0 & R^T \end{bmatrix} \tag{7}$$

where F is the force exerted by the TCA depending on its displacement, δ, and its change in temperature, q. t_a is the unit tangent vector along the TCA, and p_a is the position vector for the actuator (refer to Fig. 3). Ad_g^* properly orients the TCA wrench into the director frame. The value for δ is the arc length of the actuator minus the original length of the actuator, and in the constant strain case it is

$$\delta = \|\dot{p}_a\| L - l, \dot{p}_a = \widehat{\boldsymbol{\xi}} r \tag{8}$$

where r is the distance of the actuator from the centerline and l is the original length of the TCA.

Then, the internal wrench is only based on the stiffness of the body

$$W_{int} = K(\boldsymbol{\xi} - \boldsymbol{\xi}^*) \tag{9}$$

where K is the stiffness matrix dependent on the material properties and cross-section geometry. The $\cdot^*$ represents the value in the reference configuration. In the case of a straight cylinder $\boldsymbol{\xi}^* = [0, 0, 0, 0, 0, 1]^T$. In the simplest consideration of the stiffness, the matrix will be $K = diag(EI_x, EI_y, GJ, GA, GA, EA)$ where E is the Young's modulus, G is the shear modulus, the I's are the second area moment of inertia, J is the polar second moment of area, and A is the cross sectional area.

With the wrench balance and the constant strain assumption, we can solve the forward kinetostatics, i.e., given a change in temperature for the TCAs, we can solve the strains and thus the resulting shape of the link. All that is necessary is solving the system equations formed by the wrench balance, which can be accomplished with an equation solver such as the fsolve function in Matlab.

III. SIMULATION AND EXPERIMENTAL RESULTS

A. Materials and Fabrication

The fabrication of a shape-morphing link can be divided into three steps: (1) fabricating the TCA, (2) fabricating the

variable stiffness element, and (3) embedding the TCA and the variable stiffness element into a soft body.

We fabricate TCAs on a customized machine capable of twisting, coiling, and wrapping threads. TCAs are fabricated with silver coated nylon sewing threads (Shieldex Trading 235/35 4ply). In order to generate sufficient forces, we first twist 2 threads together by hanging a 380g weight and inserting 576 rotations per meter before self-coiling starts. To coil the twisted threads, two motors separately hold the two ends of a copper wire (with a diameter of 0.4 mm), keeping it taut and rotate to coil the threads in heterochirality (i.e., coiling and twisting have opposite directions) [18]. Preventing untwist and stabilizing the actuator are done through annealing in an oven (Quincy Lab 10GCE) for 2 hours at a constant temperature of 160°C. The outer and inner diameter of the TCA are 1.4 mm and 0.4 mm, respectively. The diameter of the twisted fiber in the TCA is 0.5 mm.

For the variable stiffness element, we wrap resistance wires (UXCELL Nichrome, diameter 0.1 mm) on a PLA rod (HATCHBOX PLA 3D Printer Filament, diameter 1.75 mm), acting as a shape-holding element.
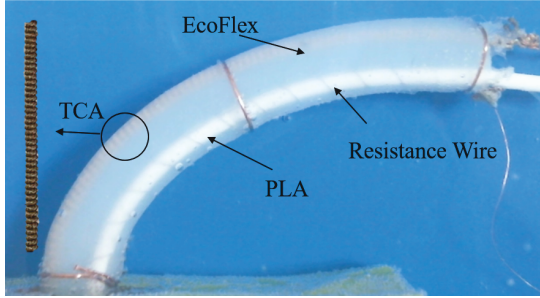

Fig. 4: The fabricated shape-morphing link

The TCA and the variable stiffness element are arranged into 3D printed molds. Then degassed EcoFlex 00-10 (Smooth-On Inc.) is poured into the assembled mold from vent holes. Finally, after 4 hours of curing, the link is demolded and the copper wire inside the TCA is pulled out. The shape-morphing link with all components labeled is shown in Fig. 4.

B. Measuring Convection Heat Transfer Coefficient

Due to the large value of the heat transfer coefficient h underwater, the steady state can be reached much faster than in free air or forced air, and thus facilitate our experiments. In this paper, we only verify our model through underwater experiments.

The shape-morphing link dissipates energy to the surroundings through its boundary, and the convective heat transfer coefficient h is critical to get the temperature of the TCA. However, this critical value is not available in existing literature and approximating it from similar materials might cause errors. So, we experimentally measured the coefficient as follows.

The procedure consists of three steps: (1) measuring temperature at the surface of a link, (2) calculating h, and (3) verifying h. It's a complicated task to measure the temperature at the surface of the body made of EcoFlex-00-10 material because contactless methods such as thermal cameras and lasers cannot accurately measure the temperature for a transparent material [19]. In this case, we fabricated a cylinder with EcoFlex 00-10 embedded with a resistance wire (UXCELL Nichrome, diameter 0.1 mm) of a helical shape with a diameter of 2 mm at the center of the body and embedded three thermistors into the soft body, which are located as shown in Fig. 5. The diameter and length of the cylinder are $D_h = 20$ mm, $L_h = 115$ mm, respectively.
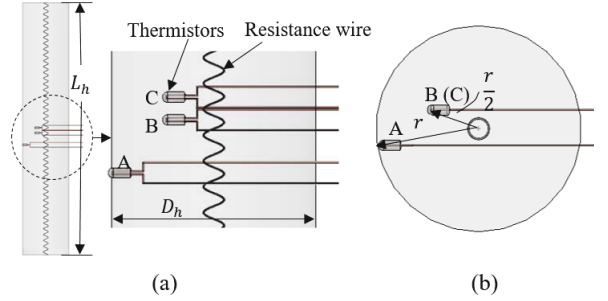

(a)   (b)

Fig. 5: Experimental setup to measure the convective heat transfer coefficient h. (a) The detailed front view. (b) The cross-section view.

The heating rate of the resistance wire can be calculated from the voltage U and resistance of the heating wire R. Thermistor A indicates the temperature at the surface (T_s), and the thermistor B and C indicates the temperature at the center of the cylinder. An Arduino Uno board is used to sample data from the thermistors. We can calculate the convective heat transfer coefficient h from

$$h = \frac{U^2}{R \pi D_h L_h (T_s - T_\infty)} \tag{10}$$

where R is the resistance for the resistive wire. The temperature of the center (B and C) can be calculated from

$$T_m = \frac{U^2}{R} \frac{\ln(2)}{2 \pi k_e L_h} + T_s \tag{11}$$

where k_e is the thermal conductivity of EcoFlex-00-10.

The average value of nine measurements for h is 101.3 W/(m²·K). We can compare the analytical result of temperatures at B and C with the thermistor readings to verify the estimation of h. Also the h is accurate only when the measured temperatures at B and C coincide with the value calculated from Eq. (11). Comparisons between the calculation result and the reading of the thermistors B and C are shown in Fig. 6. The analytical results differ from the reading value by 5%, suggesting the direct measurement method provides a precise estimation of h. The difference between B and C thermistors might be caused by inaccurate placements inside the EcoFlex material.
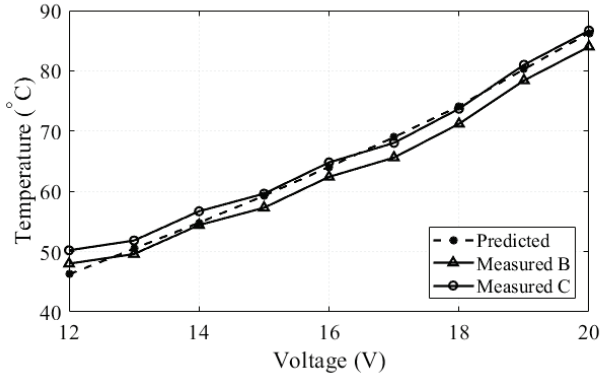
Fig. 6: Experimental and analytical results of temperatures at the middle point (B and C) to verify the correctness of h.

Fig. 8: Powers applied on the TCA and PLA rod with respect to time

C. Verification of the Model in Water.

Through the proposed model discussed in section II, we can predict a series of steady-state radii of the link from corresponding input powers. First, simulations of the thermal model are conducted with material properties of EcoFlex-00-10, and the PLA rod related to the heat transfer process, as shown in Table I. Then, the resulting temperatures from thermal simulations are passed into the kinetostatic model to get the corresponding radius.

TABLE I: PROPERTY OF PLA, TCA, AND ECOFLEX

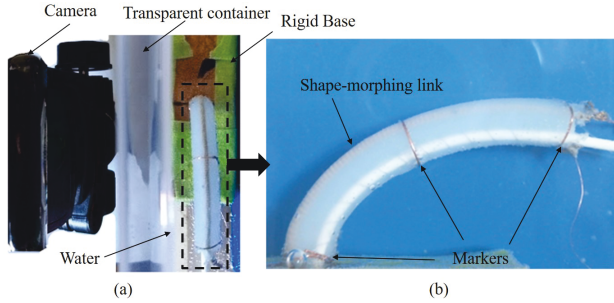| materials	k (W·m^{-1}·K^{-1})	ρ (kg·m^{-3})	c_p(J·kg^{-1}·K^{-1})
TCA	4.6 [1]	1300	1267
PLA [20]	0.13	1250	1200
EcoFlex	0.2 [21]	1040	1050

Fig. 7: Experimental setup for the model verification. (a) Top view. (b) View from the camera.

In the experiments, we apply a series of powers to the link and compare the radii measured and the radii predicted by the simulations. The experimental setup is shown in Fig. 7. A shape-morphing link connected to a rigid base is fixed underwater. The diameter and the length of the link are 8 mm and 50 mm, respectively. We record the link deformation with a camera placed outside a transparent container. We
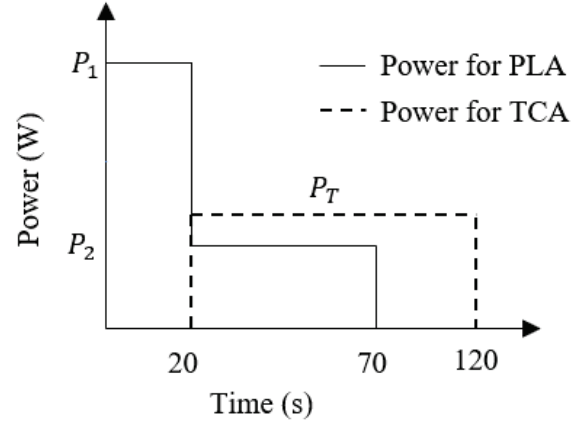
[1]The property is measured by CMC Laboratories, Inc

derive the radius of the link using its inner outline. Three thin copper wires are wrapped around the link at its two ends and middle, acting as markers that indicate the curvature of the link, which can be obtained by processing the recorded videos in Tracker (physlets.org/tracker).
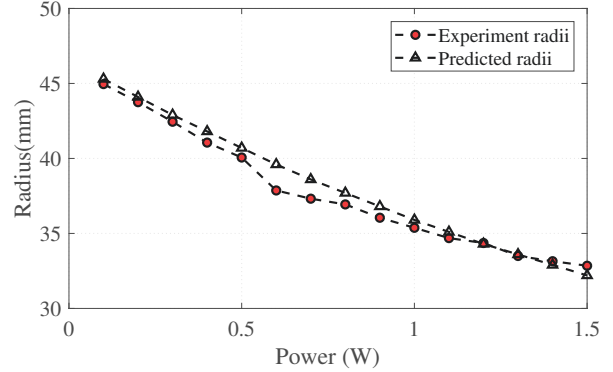

Fig. 9: Comparison of the radii obtained in experiments and simulation prediction

In the experiment, we apply the power to the PLA and the TCA as shown in Fig. 8. First, we heat the resistance wire with $P_1 = 4$ W for 20 seconds, and after the PLA is soft, reduce the power to $P_2 = 1.5$ W to keep it soft. Then we apply power to the TCA. When the shape-morphing link reaches its final position, the voltage applied to the resistance wire is removed, allowing the PLA to become rigid again. We did the experiments with a series of input powers for the TCA from 0.1 W to 1.5 W with a step size of 0.1 W.

The radii of the shape-morphing link from the experiments are plotted against a series of powers applied to the TCA and compared with the radii predicted by simulations in Fig. 9. From the figure, the two lines generally agree with each other. The main error is likely caused by the pre-bending of the link, meaning the link cannot recover to its completely straight position even at room temperature. The

second reason for the difference is that the stiffness of the PLA influences the deformation of the body, but it is not included in the model.

IV. APPLICATION

We demonstrate that the shape-morphing link can replace one of the normal links in a four-bar mechanism to alter the trajectory of its foot. The two ends of the PLA rod are directly plugged into the holes designed in the joints to facilitate our assembly process. A miniature DC motor (Part #: GH612s from Gizmozone) drives the linkage. We attach the linkage to the wall of the container filled with water and we do so in a way that leaves the linkage fully submerged except for the motor. The morphing sequence is the same
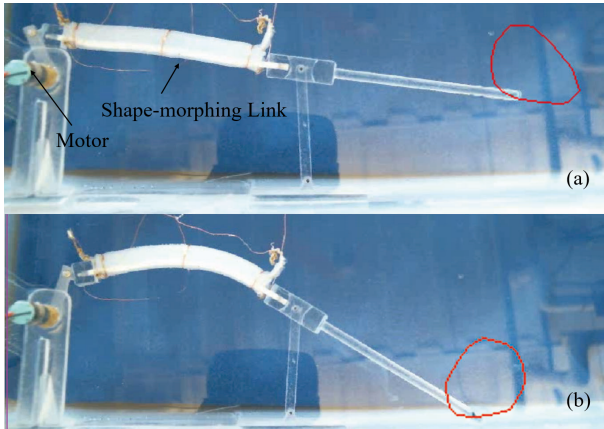

Fig. 10: Configuration and trajectory (curves in red color) comparison (a) Before shape morphing. (b) After shape morphing. A video is available at: https://youtu.be/RK1Jnvfy6J4

with the verification experiment. An input power of 0.5 W is applied to the TCA. After shape morphing, the bending of the morphing link leads to a different foot trajectory when the linkage is actuated. The comparison of the two configurations and their trajectories is shown in Fig. 10.

With the configurations before and after the shape morphing, we show that the resultant trajectory will not only change its shape but also its location. Although a simple four-bar mechanism with one shape morphing link is demonstrated, we expect that this can be leveraged for altering the gaits for walking robots on-the-fly without modifying the mechanism [22].

V. CONCLUSIONS

We have developed a shape-morphing link actuated by a TCA, which can move and hold a new configuration without energy input. A model consisting of a kinetostatic model and a thermal model is developed to directly relate input power and the shape-morphing link's final configuration. The model can predict the resulting radius of the shape-morphing link, which is verified by comparisons between the predicted radii and the radii measured in experiments. The morphing link is applied to change the foot trajectory of a four-bar linkage, suggesting this new shape-morphing scheme can

potentially increase functionality and adaptability for future robotic designs.

REFERENCES

[1] S. Mintchev and D. Floreano, "Adaptive morphology: A design principle for multimodal and multifunctional robots," *IEEE Robotics & Automation Magazine*, vol. 23, no. 3, pp. 42–54, 2016.

[2] A. A. Paranjape, S.-J. Chung, and J. Kim, "Novel dihedral-based control of flapping-wing aircraft with application to perching," *IEEE Transactions on Robotics*, vol. 29, no. 5, pp. 1071–1084, 2013.

[3] Y. She, C. J. Hurd, and H.-J. Su, "A transformable wheel robot with a passive leg," in *Intelligent Robots and Systems (IROS), 2015 IEEE/RSJ International Conference on*. IEEE, 2015, pp. 4165–4170.

[4] A. Tonazzini, S. Mintchev, B. Schubert, B. Mazzolai, J. Shintake, and D. Floreano, "Variable stiffness fiber with self-healing capability," *Advanced Materials*, vol. 28, no. 46, pp. 10 142–10 148, 2016.

[5] W. Shan, T. Lu, and C. Majidi, "Soft-matter composites with electrically tunable elastic rigidity," *Smart Materials and Structures*, vol. 22, no. 8, p. 085005, 2013.

[6] W. Shan, S. Diller, A. Tutcuoglu, and C. Majidi, "Rigidity-tuning conductive elastomer," *Smart Materials and Structures*, vol. 24, no. 6, p. 065001, 2015.

[7] M. C. Yuen, R. A. Bilodeau, and R. K. Kramer, "Active variable stiffness fibers for multifunctional robotic fabrics," *IEEE Robotics and Automation Letters*, vol. 1, no. 2, pp. 708–715, 2016.

[8] NinjaTek PLA 3D printing filament. [Online]. Available: https://ninjatek.com/wp-content/uploads/2016/05/PLA-TDS.pdf

[9] M. McEvoy and N. Correll, "Shape change through programmable stiffness," in *Experimental Robotics*. Springer, 2016, pp. 893–907.

[10] T. L. Buckner, E. L. White, M. C. Yuen, R. A. Bilodeau, and R. K. Kramer, "A move-and-hold pneumatic actuator enabled by self-softening variable stiffness materials," in *2017 IEEE/RSJ International Conference on Intelligent Robots and Systems (IROS)*, Sept 2017, pp. 3728–3733.

[11] C. S. Haines, M. D. Lima, N. Li, G. M. Spinks, J. Foroughi, J. D. Madden, S. H. Kim, S. Fang, M. J. de Andrade, F. Göktepe, *et al.*, "Artificial muscles from fishing line and sewing thread," *science*, vol. 343, no. 6173, pp. 868–872, 2014.

[12] J. Zhao and A. Abbas, "A low-cost soft coiled sensor for soft robots," in *ASME 2016 Dynamic Systems and Control Conference*. American Society of Mechanical Engineers, 2016, pp. V002T26A006–V002T26A006.

[13] T. L. Bergman and F. P. Incropera, *Fundamentals of heat and mass transfer*. John Wiley & Sons, 2011.

[14] M. C. Yip and G. Niemeyer, "On the control and properties of supercoiled polymer artificial muscles," *IEEE Transactions on Robotics*, vol. 33, no. 3, pp. 689–699, 2017.

[15] A. Abbas and J. Zhao, "Twisted and coiled sensor for shape estimation of soft robots," in *2017 IEEE/RSJ International Conference on Intelligent Robots and Systems (IROS)*, Sept 2017, pp. 482–487.

[16] ——, "A physics based model for twisted and coiled actuator," in *Robotics and Automation (ICRA), 2017 IEEE International Conference on*. IEEE, 2017, pp. 6121–6126.

[17] D. C. Rucker and R. J. W. III, "Statics and dynamics of continuum robots with general tendon routing and external loading," *IEEE Transactions on Robotics*, vol. 27, no. 6, pp. 1033–1044, Dec 2011.

[18] A. N. Semochkin, "A device for producing artificial muscles from nylon fishing line with a heater wire," in *Assembly and Manufacturing (ISAM), 2016 IEEE International Symposium on*. IEEE, 2016, pp. 26–30.

[19] M. Vollmer, M. Klaus-Peter, *et al.*, *Infrared thermal imaging: fundamentals, research and applications*. John Wiley & Sons, 2017.

[20] B. Mortazavi, F. Hassouna, A. Laachachi, A. Rajabpour, S. Ahzi, D. Chapron, V. Toniazzo, and D. Ruch, "Experimental and multiscale modeling of thermal conductivity and elastic properties of pla/expanded graphite polymer nanocomposites," *Thermochimica Acta*, vol. 552, pp. 106–113, 2013.

[21] M. D. Bartlett, N. Kazem, M. J. Powell-Palm, X. Huang, W. Sun, J. A. Malen, and C. Majidi, "High thermal conductivity in soft elastomers with elongated liquid metal inclusions," *Proceedings of the National Academy of Sciences*, p. 201616377, 2017.

[22] A. DeMario and J. Zhao, "Development and analysis of a three-dimensional printed miniature walking robot with soft joints and links," *Journal of Mechanisms and Robotics*, vol. 10, no. 4, p. 041005, 2018.